RSC Advances

PAPER

View Article Online
View Journal | View Issue

Cite this: *RSC Adv.*, 2025, **15**, 40231

Fabrication of a strong, tough, recyclable, and multifunctional bio-based epoxy vitrimer *via* constructing polyarylation-enhanced dynamic networks

Zhiwei Chang, *[ab] Xiaochun Bao,[ab] Guimin Yuan,[ab] Yuang Ma,[ab] Ming Li[ab] and Hanjie Ying [ab]

Received 4th September 2025
Accepted 11th October 2025

DOI: 10.1039/d5ra06660c

rsc.li/rsc-advances

The fabrication of eco-friendly bio-based epoxy resins is of critical importance for addressing the excessive consumption of petroleum resources and the release of harmful substances caused by petroleum-based thermosetting epoxy resins. However, the non-recyclability and poor mechanical properties of bio-based epoxy resins hinder their further development and application. Herein, a strong, tough, recyclable, and multifunctional bio-based epoxy vitrimer is prepared using epoxidized soybean oil (ESO) and lignin-based aromatic monomers of vanillyl alcohol, guaiacol, and vanillin. These lignin-based aromatic monomers provide bio-based aromatic building blocks for the synthesis of bisguaiacol F diamine vanillin (BGAV) with dynamic imine bonds, which is employed as a curing agent for ESO to fabricate a bio-based epoxy vitrimer incorporating a dynamic network. The BGAV forms rigid polyaromatic segments in the network to enhance the stability of the polymer, thereby leading to a high mechanical strength of 21.81 MPa for the epoxy vitrimer. Moreover, the hydrogen bonds in the network serve as sacrificial bonds to increase the ability of energy dissipation, thereby resulting in excellent toughness of 27.53 MJ m^{-3} for the epoxy vitrimer. Additionally, the reversible reconstruction of dynamic imine bonds within the network endows the vitrimer with favorable self-healing properties and recyclability. Furthermore, the vitrimer also exhibits outstanding antibacterial properties, mold resistance, photothermal conversion performance, water resistance, and bonding performance. This work provides an effective approach for the development of recyclable bio-based epoxy resins with exceptional mechanical properties and multifunctionality.

1. Introduction

Thermosetting epoxy resins are widely used in adhesives, coatings, and electronic packaging due to their excellent mechanical properties, chemical resistance, and thermal stability.[1,2] However, petroleum-based bisphenol A epoxy resins account for more than 90% of the market share for these epoxy resins, leading to the excessive consumption of petroleum resources and the release of harmful substances such as bisphenol A.[3,4] Seeking nontoxic, renewable, bio-based epoxy resins as alternatives to bisphenol A epoxy resins undoubtedly represents one of the most promising approaches to solving the aforementioned problems.[5,6] Soybean oil, castor oil, and tung oil-based epoxy resins have attracted increasing attention as potential candidates.[7–9] Among them, soybean oil-based epoxy resins have become a research hotspot due to their abundant raw materials, simple processing, and low cost.[10,11] Nevertheless, these epoxy resins after curing typically form permanent polymer networks that cannot be repaired or recycled once the resin is damaged or fails, resulting in resource waste and environmental burden.[12]

Covalent adaptive networks (CANs) are dynamic networks constructed by dynamic covalent bonds.[13,14] A range of dynamic covalent bonds such as imine bonds,[15] boronic esters,[16] disulfide linkages,[17] hydroxyl esters[13] and Diels–Alder,[18] have been engineered into epoxy resins. Epoxy vitrimers based on dynamic covalent bonds attract significant research interest due to their reversible crosslinking and exceptional reusability.[14,16] In recent years, soybean oil-based epoxy vitrimers have achieved notable progress, demonstrating remarkable recyclability and processability. Hu *et al.* utilized epoxidized soybean oil (ESO) to fabricate a multi-stimuli response, self-healing, and recyclable bio-based vitrimer *via* constructing a dynamic ester bond network.[19] Wang *et al.* used ESO to prepare a recyclable superhydrophobic coating with dynamic imine bonds.[20] However,

---

[a] *College of Biotechnology and Pharmaceutical Engineering, Nanjing Tech University, No. 30, Puzhu South Road, Nanjing, 211816, China. E-mail: changzhiwei@njtech.edu.cn*

[b] *State Key Laboratory of Materials-Oriented Chemical Engineering, No. 30, Puzhu South Road, Nanjing, 211816, China*

soybean oil-based epoxy vitrimers demonstrate inferior mechanical properties and thermal stability due to the inherent instability of dynamic covalent bonds. Thus, developing soybean oil-based epoxy vitrimers that simultaneously exhibit superior mechanical properties and recyclability presents significant challenges. Curing agents are essential components in the synthesis of epoxy resins.[21,22] Notably, incorporating rigid aromatic curing agents into epoxy resins provides an effective method for enhancing their mechanical properties. Jiao *et al.* employed 4,4-dithiodianiline and sebacic acid as co-curing agents to prepare a high-strength epoxy vitrimer.[23] Li *et al.* developed a series of diphenyl diamino curing agents for significantly enhancing the thermal stability and mechanical strength of epoxy resins.[24] However, the majority of these aromatic curing agents originate from non-renewable petroleum-based monomers. Lignin ranks as the third most abundant renewable polymer, which constitutes 20–30% of lignocellulosic components.[25] The aromatic monomers derived from lignin depolymerization provide bio-based aromatic building blocks for manufacturing epoxy curing agents.[26,27] Consequently, employing lignin-based aromatic monomers to synthesize bio-based curing agents with dynamic covalent bonds for soybean oil-based epoxy vitrimers is expected to prepare bio-based, high-strength, and recyclable epoxy resins.

Herein, bisguaiacol F diamine vanillin (BGAV) with dynamic imine bonds was synthesized using lignin-based aromatic monomers including vanillyl alcohol, guaiacol, and vanillin (Fig. 1a). The BGAV was then employed as a bio-based curing agent for ESO to prepare a strong, tough, recyclable, and multifunctional bio-based epoxy vitrimer (ESO/BGAV) (Fig. 1b). Interestingly, the BGAV formed rigid polyaromatic segments within the polymer network, resulting in the high mechanical strength of ESO/BGAV. Meanwhile, the hydrogen bonds (H-bonds) within the network acted as sacrificial bonds, increasing the energy dissipation of the system and thereby causing the great toughness of ESO/BGAV. Moreover, the dynamic imine bonds within the network imparted ESO/BGAV with excellent self-healing properties and recyclability by their dynamic reconfiguration. Additionally, the antimicrobial effect of the imine bonds endowed ESO/BGAV with favorable antibacterial properties and mold resistance. Furthermore, the polyaromatic segments within the system served as conjugated structures and hydrophobic groups, leading to the significant photothermal conversion capability and water resistance of

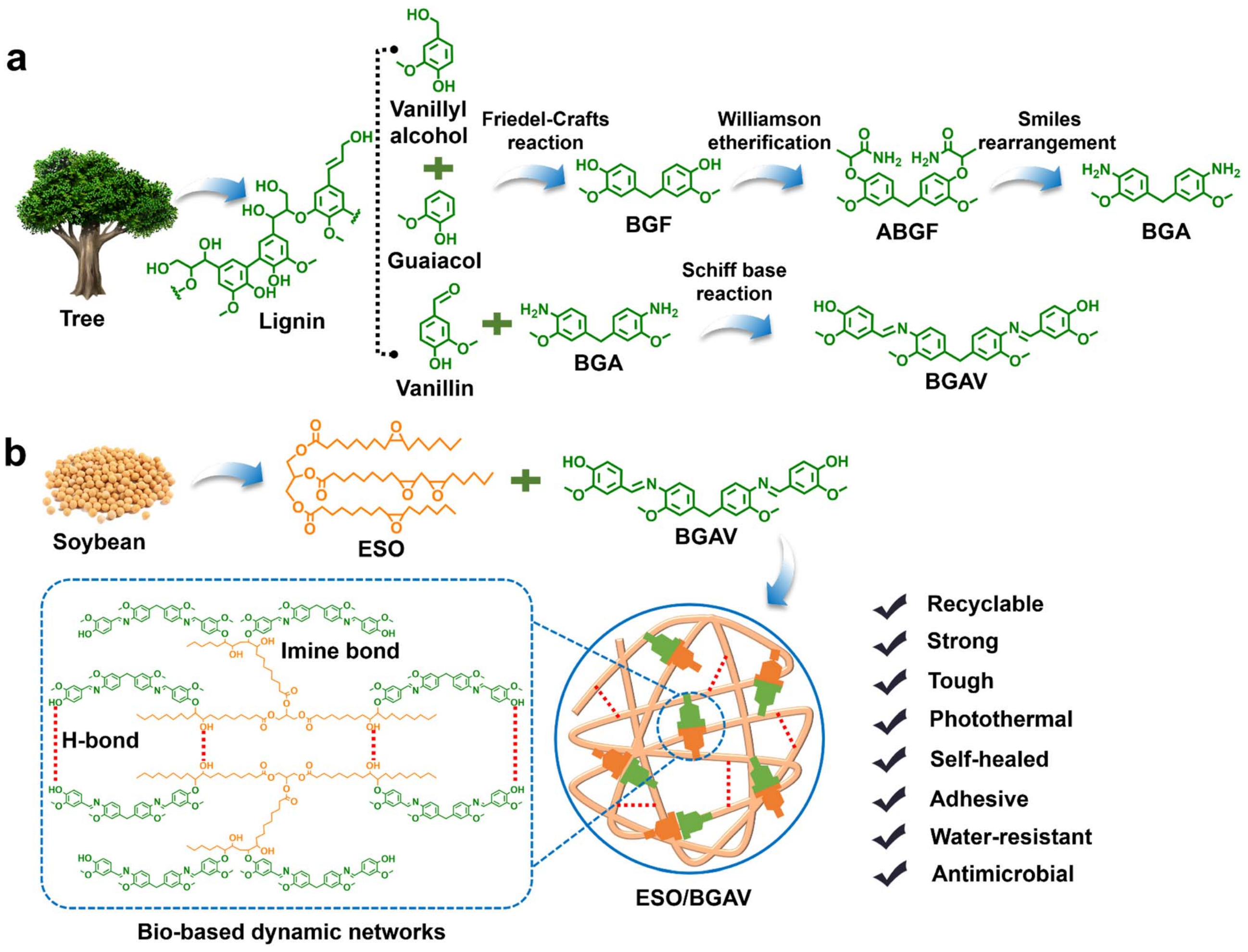

Fig. 1 (a) Synthesis of BGAV and (b) fabrication of ESO/BGAV epoxy vitrimer.

ESO/BGAV. It was noteworthy that ESO/BGAV displayed outstanding bonding performance when used as an adhesive, which originated from the balance between the cohesive force of the polymer and its interfacial force with the substrates. This structural design presents a sustainable and viable method for fabricating strong and tough recyclable bio-based epoxy resins.

2. Experimental section

2.1. Materials

ESO (epoxy value was 6.76%, epoxy equivalent weight was 236.86 g per eq.), vanillyl alcohol, guaiacol, and vanillin were provided by Tianjin Heowns Biochemical Technology Co., Ltd. Ethyl alcohol, H_2SO_4, ethyl acetate, petroleum ether, KI, K_2CO_3, KOH, DMSO, CH_2Cl_2, THF, HCl, toluene, dichloromethane (DCM), and silicone oil was ordered from Shanghai Aladdin Biochem Co., Ltd. Acetone, cyclohexane, 2-bromopropionamide, DMPU, 1,4-dioxane, 4-dimethylaminopyridine, and (DMAP) was supplied by Shanghai Sinopharm Chemical Reagent Co., Ltd.

2.2. Synthesis of bisguaiacol F (BGF)

3.04 g of vanillin and 2.48 g of guaiacol were introduced into 200 mL of ethyl alcohol and stirred thoroughly. Subsequently, 5 mL of H_2SO_4 solution (0.25 mol L^{-1}) was added to the above solution and stirred at 100 °C for 36 h. After cooling to room temperature, the solvent was removed by rotary evaporation and was purified by using ethyl acetate and petroleum ether to obtain BGF with a yield of 89%.

2.3. Synthesis of alkylated BGF (ABGF)

5 g of BGF, 0.32 g of KI, 7.96 g of K_2CO_3, and 5.8 g of 2-bromopropionamide were added sequentially to 150 mL of acetone. Then, the mixture was reacted at 80 °C and refluxed for 24 h. After cooling to room temperature, the mixture was concentrated under reduced pressure using a rotary evaporator. Additionally, the mixture was purified by using ethyl acetate and cyclohexane as the eluent to afford ABGF with a yield of 94% after vacuum drying at 45 °C.

2.4. Synthesis of bisguaiacol F diamine (BGA)

5 g of ABGF and 1.67 g of KOH were introduced into 100 mL of the mixed solvent of DMSO and DMPU. The volume ratio of DMSO and DMPU was 3 to 1. The mixture was stirred continuously at 180 °C for 3 h. After cooling to room temperature, the reaction mixture was diluted 2.5-fold with deionized water and then extracted three times with ethyl acetate. The mixture was purified using ethyl acetate and petroleum ether as the eluent and was further vacuum-dried at 45 °C to obtain BGA with a yield of 68%.

2.5. Synthesis of BGAV

2.4 g of BGA and 2.8 g of vanillin were added to 50 mL of ethyl alcohol, which was stirred at 80 °C for 12 h under a nitrogen atmosphere. After cooling to room temperature, the mixture was left to stand overnight, followed by the separation of the solvent from the precipitate. Subsequently, the precipitation was washed three times with ethyl acetate and vacuum-dried at 80 °C for 12 h to afford BGAV with a yield of 83%. The molecular weight of BGAV was 542.63 Da. The hydroxyl value of BGAV was 6.27%.

2.6. Fabrication of ESO/BGAV epoxy vitrimer

1 g of ESO was blended respectively with different amounts (0.8, 1.0, 1.2, 1.4, and 1.6 g) of BGAV in 5 mL of 1,4-dioxane. The five different stoichiometric molar ratios of hydroxyl to epoxy groups were 0.70, 0.875, 1.05, 1.225, and 1.40. Then, the 0.02 g of DMAP as a catalyst was introduced into the mixed solution, followed by stirring at 25 °C for 30 min under a nitrogen atmosphere. Further, the mixed solution was transferred into a mold and cured at 140 °C for 3 h under vacuum drying to obtain a series of ESO/BGAV epoxy vitrimer. The five vitrimers with different BGAV contents were designated as ESO/BGAV-1, ESO/BGAV-2, ESO/BGAV-3, ESO/BGAV-4, and ESO/BGAV-5 (Table S1).

2.7. Preparation of ESO/BGAV epoxy vitrimer adhesive

The pre-cure ESO/BGAV epoxy vitrimer was employed as a bio-based adhesive. Specifically, 1 g of ESO and different amounts (0.8, 1.0, 1.2, 1.4, and 1.6 g) of BGAV were introduced into 5 mL of 1,4-dioxane. Subsequently, the 0.02 g of DMAP was added into the mixed solution and stirred at 25 °C for 30 min under a nitrogen atmosphere to obtain a series of ESO/BGAV epoxy vitrimer adhesives.

2.8. Characterization

Fourier transform infrared (FTIR) spectra were obtained using a Nicolet 7600 spectrometer (Thermo Fisher Scientific, USA). Temperature-dependent FTIR spectra were measured *in situ* over a temperature range of 40 to 220 °C. ^1H nuclear magnetic resonance (NMR) spectra were recorded on a JNM-ECZ600R spectrometer (JEOL, Japan). X-ray photoelectron spectroscopy (XPS) spectra were measured using an ESCALAB 250Xi X-ray photoelectron spectrometer (Thermo Fisher Scientific, USA). Thermogravimetry (TG) analysis was conducted on a STA 409 PC thermal analyzer (NETZSCH, Germany). Differential Scanning Calorimetry (DSC) tests were carried out using a DSC 300 Classic instrument (Netzsch, Germany). The samples were heated from −75 °C to 200 °C at a rate of 10 °C min^{-1} in a N_2 atmosphere at a flow rate of 50 mL min^{-1}. Dynamic mechanical analysis (DMA) was performed on a Discovery DMA 850 system (TA Instruments, USA). Specimens for testing were prepared by cutting the 1.2 ± 0.05 mm thick films into 6 mm × 10 mm strips. The viscoelastic characterization was conducted *via* a same frequency sweep at 1 Hz. The test consisted of applying an oscillatory strain of 0.1% within a temperature range of 10 °C to 170 °C. Water contact angle (CA) was measured by a HARKESPCAX3 instrument (HARKE Test Instrument Factory, China). The fractured surface of the films was observed by a scanning electron microscope (SEM, Hitachi S-3400N, Japan).

2.9. Swelling ratio measurement

The vitrimer sample was weighed to obtain its initial mass (m_1), followed by immersion in DI water. The weight of the swollen sample (m_2) was weighed every day. The swelling ratio was calculated using the following equations:

$$\text{Swelling ratio (\%)} = (m_2 - m_1)/m_1 \times 100 \tag{1}$$

2.10. Mechanical performance measurement

The vitrimer films were cut into samples with a size of 10 mm × 80 mm and then were put on an AGS-X tensile testing machine (Shimadzu, Japan) for measuring the mechanical performance. Parameters were set to 50 mm initial gauge length and 20 mm min^{-1} loading speed. The measurement of each sample was repeated at least 6 times. Tensile cycling tests and tensile loading-unloading tests were conducted under identical conditions. The films were cut into trouser-shaped specimens (50 mm × 8 mm with a 20 mm notch) for tear tests on the tensile testing machine at a stretching speed of 50 mm min^{-1}.

2.11. Photothermal performance measurement

The photothermal performance of the vitrimer film was measured using a home-made photothermal test setup consisting of an infrared laser (808 nm, 1 W cm^{-2}) and an E60 infrared thermal imager (FLIR, USA).

2.12. Self-healing properties measurement

Scratches at 50–70% depth were created on the film samples with a blade. The scratched film was placed 10 cm beneath a 1 W cm^{-2} infrared laser for 10 minutes, while its self-healing process was observed with an optical microscope.

2.13. Recyclability measurement of film

For physical recycling, the prepared vitrimer film was mechanically ground into powder, and subsequently the powder was hot pressed at 140 °C and 5 MPa for 20 min to obtain recycled vitrimer films. For chemical recycling, the prepared film was depolymerized by immersing it in a CH_2Cl_2/THF/HCl mixed solvent (pH = 1.3). The volume ratio of CH_2Cl_2, THF, and HCl was 10 : 10 : 1. Then, the mixture was shaken at 25 °C for 6 hours to obtain a depolymerized solution. After extraction with DCM and rotary evaporation, the small molecule polymer was obtained. A certain amount of 1,4-dioxane was used as the solvent for the small molecule polymer, which was poured into a mold and dried to obtain the recovered film.

2.14. Adhesion performance, bonding performance, and water resistance measurement of ESO/BGAV adhesive

The lap samples were prepared by uniformly coating the surfaces of different substrates with the prepared vitrimer adhesives at an application rate of 150 g m^{-2}. The adhesion area was 25 × 25 mm. After being maintained at room temperature for 1 h, the adhesion strength of lap samples was obtained by testing the lap samples on a universal mechanical machine at a crosshead speed of 10 mm min^{-1}. Additionally, the prepared vitrimer adhesives were evenly spread on different substrates at an application rate of 150 g m^{-2} with a bonding area of 25 × 25 mm of the bonding area to prepare lap samples. After being cured at 140 °C for 6 min, the samples were tested on a universal testing machine to obtain bonding strength. Moreover, the above-prepared cured lap specimens were immersed in 63 °C water for 3 h and then were tested on a universal tensile testing machine at a test speed of 10 mm min^{-1} at a crosshead speed of 10 mm min^{-1}. The dimensions of specimens of adhesion performance, bonding performance, and water resistance measurements are shown in Fig. S1.

2.15. Recyclability of ESO/BGAV adhesive

For physical recycling, the two separated iron substrates coated with adhesive after lap shear tests were re-joined and clamped. The sample was placed at 140 °C for 6 min and was then tested on a universal testing machine at a test speed of 10 mm min^{-1}. For chemical recycling, the process was similar to the chemical recycling of vitrimer film. 1.6 g of the obtained small molecule polymer was mixed with 5 mL of 1,4-dioxane and vigorously stirred to yield the recycled adhesive. The recycled adhesive was uniformly spread on the iron substrates for preparing the lap samples. The lap samples were measured on a universal testing machine at a test speed of 10 mm min^{-1}.

2.16. Antimicrobial properties of ESO/BGAV adhesive

For antibacterial properties tests, the vacuum-dried vitrimer was ground into a 200-mesh powder, which was prepared into a vitrimer solution at a concentration of 20 mg mL^{-1} using sterile water. Bacterial suspensions (5×10^4 CFU mL^{-1} in PBS) were combined with the vitrimer solution and then incubated at 37 °C for 4 h. After a 10-fold serial dilution, 40 μL of the mixed solution was spread on LB agar plates and incubated at 37 °C for 24 h. Bacterial viability was determined from colony counts. For mold resistance tests, the wood veneers coated with vitrimer adhesive in both uncured and cured states were placed in a condition of 30 °C and 90% RH. The mold resistance was evaluated by observing the fungal growth on the surface of the samples.

3. Results and discussion

3.1. Fabrication and characterization of ESO/BGAV

To fabricate ESO/BGAV with a dynamic network, BGAV containing dynamic covalent bonds was first synthesized using lignin-based aromatic monomers. BGF was synthesized from vanillyl alcohol and guaiacol *via* a Friedel–Crafts reaction with a yield of 89%. ABGF was obtained *via* Williamson etherification of BGF with a 94% yield, followed by conversion to BGA through Smiles rearrangement in 68% yield. BGA was graft-modified with vanillin *via* the Schiff base reaction to prepare BGAV with dynamic imine bonds, and the yield was 83%. The chemical structure of the BGAV was characterized using ^{1}H NMR spectroscopy. As shown in Fig. S2a–d, compared to the ^{1}H NMR spectrum of BGF, new signal peaks (1.63, 4.62, 7.29 ppm) attributable to the propionamide group emerged in the ^{1}H NMR spectrum of ABGF, while the characteristic peak (9.79 ppm) corresponding to the phenolic hydroxyl group disappeared. This confirmed that the propionamide groups have grafted onto ABGF *via* Williamson etherification of the phenolic hydroxyl groups of BGF.[28] Additionally, compared to the ^{1}H NMR spectrum of BGA, the new signal peaks (3.85, 6.83, 7.29, 7.66, 8.38, and 9.82 ppm) corresponding to the structure of vanillin were detected, and the signal peak (4.95 ppm) corresponding to the amine group disappeared in that of BGAV. This indicated that vanillin was grafted onto BGA through the Schiff base reaction.[29] Further, BGAV served as a bio-based curing agent for ESO to synthesize the ESO/BGAV epoxy vitrimers. The chemical structure of the ESO/BGAV was studied by FTIR and XPS. As shown in Fig. 2a, the epoxy group peak (841 cm^{-1}) in the FTIR spectra of ESO disappeared in that of ESO/BGAV. Meanwhile, a new alcoholic hydroxyl peak (3386 cm^{-1}) was observed in the spectra of ESO/BGAV. This indicated that ESO and BGAV underwent polymerization through an epoxy ring-opening reaction and generated alcoholic hydroxyl groups.[30] The C=N peak in FTIR spectra of BGAV (1623 cm^{-1}) was also found in that of ESO/BGAV (1626 cm^{-1}), suggesting that the dynamic imine bonds in BGAV are retained in the ESO/BGAV system.[20] Besides, compared with positions of the ester carbonyl peak (1737 cm^{-1}) and aliphatic –CH$_2$– peak (2922 cm^{-1}) in spectra of ESO, these peaks shifted to 1741 cm^{-1} and 2925 cm^{-1} in that of ESO/BGAV, indicating the formation of H-bonds within the network of ESO/BGAV.[31] The XPS spectrum is shown in Fig. S3. Compared to the C 1s spectrum of ESO, a new C=N peak was detected in ESO/BGAV. Simultaneously, this C=N peak was also observed in the C 1s spectrum of BGAV, further confirming the incorporation of dynamic imine bonds into the structure of ESO/BGAV.[32]

The thermal stability of ESO/BGAV was studied by TG and DSC. As shown in Fig. 2b, the residual carbon ratio in the TG curves of ESO/BGAV first rose and then declined as the addition amount of BGAV gradually increased. The residual carbon ratio of ESO/BGAV-3 increased from 13.46% of ESO/BGAV-1 to 16.67%. $T_{95\%}$ in TG curves corresponded to the temperature at which the degradation reached 5% of the original mass. The $T_{95\%}$ of ESO/BGAV-3 improved from 298.43 °C of ESO/BGAV-1 to 310.84 °C. Moreover, the thermal degradation peaks in the DTG curves of ESO/BGAV displayed an initial decrease followed by an increase with rising BGAV content (Fig. 2c). The first and second thermal degradation peak rates of ESO/BGAV-3 decreased to 0.68%/°C and 0.62%/°C, respectively, compared to 0.79%/°C and 0.75%/°C for ESO/BGAV-1. These results of TG tests suggested that the addition of an appropriate amount of BGAV enhanced the thermal stability of the crosslinked network in ESO/BGAV.[33] The molar ratio of hydroxyl to epoxy groups for ESO/BGAV-3 was close to 1 : 1, which was an optimal stoichiometric ratio to form a stable crosslinked network in ESO/BGAV. In addition, the glass transition temperatures in DSC curves of ESO/BGAV first increased and then decreased with increasing BGAV content (Fig. 2d), and that of ESO/BGAV-3 improved from 73 °C to 88 °C. This result demonstrated that BGAV restricted the mobility of molecular chains in the polymer network.[20] The viscoelastic properties of the ESO/BGAV were investigated *via* DMA. As shown in Fig. 2e, the storage modulus of the ESO/BGAV also increased initially and then decreased with increasing BGAV addition, which aligned with the results from

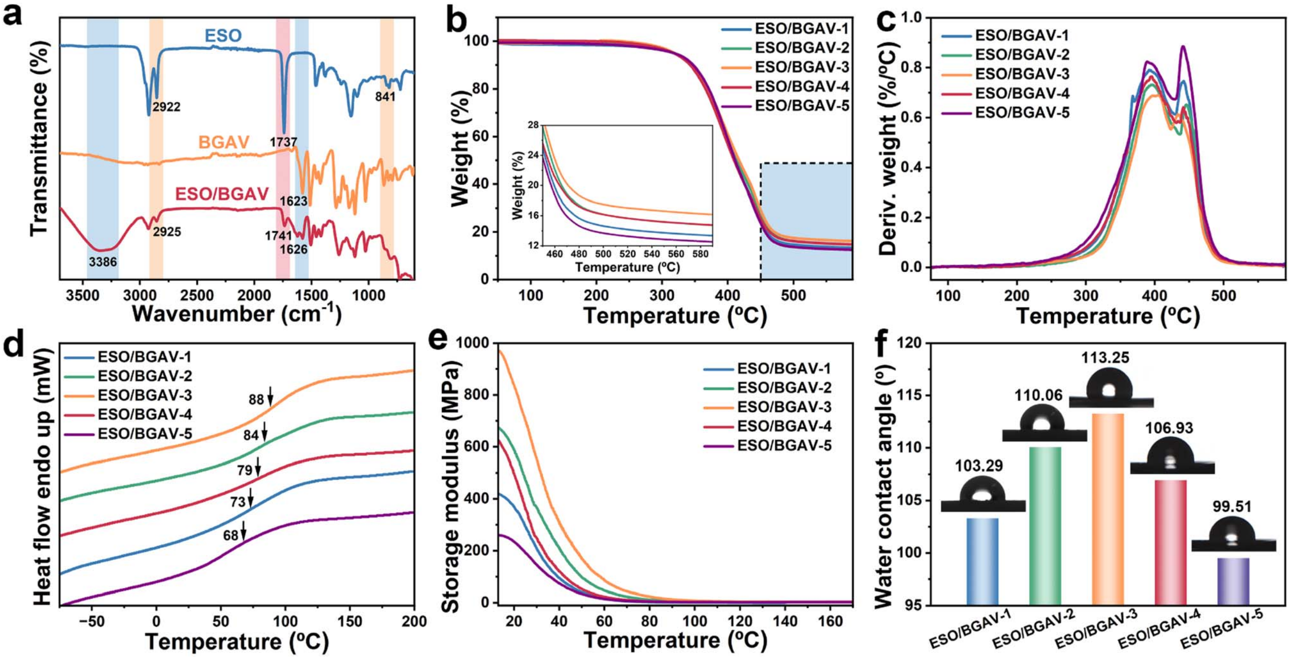

Fig. 2 (a) FTIR spectra of ESO, BGAV, and ESO/BGAV. (b) TG, (c) DTG, (d) DSC curves, (e) storage modulus, and (f) water CA of different ESO/BGAV epoxy vitrimers.

TG and DSC measurements. The storage modulus of ESO/BGAV was significantly improved by adding an appropriate amount of BGAV. This was because the polyaromatic segments of BGAV enhanced the rigidity of ESO/BGAV, thereby enhancing its resistance to stress destruction.[34,35] The crosslink density of the polymers was calculated according to the Flory's ideal rubber elasticity equation (Fig. S4). The crosslinking density of the polymers initially increased and then decreased. The ESO/BGAV-3 possessed the highest crosslinking density. The crosslinking density of ESO/BGAV-3 increases from 8458.93 mol m^{-3} of ESO/BGAV-1 to 9773.37 mol m^{-3}, demonstrating that the addition of an appropriate amount of BGAV could enhance the crosslinking density. Loss tangent (tan δ) of the ESO/BGAV was shown in Fig. S5. The trend of the glass transition temperature on the curves of tan δ was consistent with the DSC measurement results. The hydrophobicity of the ESO/BGAV was evaluated by measuring its water CA and swelling rate. As shown in Fig. 2f, the water CA of the ESO/BGAV first increased and then decreased. The water CA of ESO/BGAV-3 improved from 103.29° of ESO/BGAV-1 to 113.25°. This finding indicated that the addition of a suitable amount of BGAV improved the hydrophobicity of the polymers. The polyaromatic segments in BGAV acted as hydrophobic groups, preventing water from penetrating and damaging the crosslinking network of ESO/BGAV, thereby improving its hydrophobicity.[36,37] Nevertheless, excessive BGAV disrupted the crosslinked network of polymers, thereby reducing hydrophobicity, which resulted in a decreased water CA for ESO/BGAV-4 and ESO/BGAV-5. The swelling ratio of the ESO/BGAV initially decreased before increasing (Fig. S6). The swelling rate of ESO/BGAV-3 decreased from 26.63% of ESO/BGAV-1 to 20.57% on 7 days of immersion, which further demonstrated that the introduction of an appropriate amount of BGAV could enhance the hydrophobicity of the ESO/BGAV.

3.2. Mechanical properties of ESO/BGAV

The mechanical properties of ESO/BGAV were measured through tensile testing of ESO/BGAV films. Tensile stress–strain testing demonstrated that ESO/BGAV exhibited outstanding strength and toughness (Fig. 3a–c). The tensile strength and toughness of the ESO/BGAV were improved by optimizing BGAV content. The ESO/BGAV-3 exhibited optimal mechanical performance with a tensile strength of 21.81 MPa and toughness of 27.53 MJ m^{-3}, which represented improvements of 53.70% and 87.53% compared to the tensile strength (14.19 MPa) and toughness (14.68 MJ m^{-3}) of ESO/BGAV-1. This was because the rigidity and crosslinking strength of the polymer network in ESO/BGAV gradually improved with increasing the BGAV content at low BGAV addition levels.[38] However, when the BGAV content was excessive, the excess BGAV could not participate in the cross-linking reaction and disrupted the integrity of the network through localized defects and stress concentration, thereby reducing the strength and toughness of ESO/BGAV-5 to 11.97 MPa and 10.52 MJ m^{-3}, respectively. As shown in Fig. 3d, pronounced hysteresis loops were observed in the cyclic tensile curves of ESO/BGAV-3 (optimal ratio in ESO/BGAV), which was ascribed to the energy dissipation effect of the dense H-bonds in the polymer network.[39] Additionally, hysteresis curves of ESO/BGAV-3 at different strains were measured (Fig. 3e). An enlargement of the hysteresis loop area occurred as the strain increased, suggesting greater hysteresis loss occurs at larger strains. Hysteresis loss values per cycle at different strains were shown in Fig. S7. Hysteresis loss at lower strains was attributed to chain disentanglement of the polymer, while the breakage of H-bonds at higher strains resulted in greater hysteresis loss. It was obvious that energy dissipation persisted throughout the entire stretching process. The energy dissipation performance of ESO/BGAV-3 improved with increasing strain, which contributed to its excellent durability. The influence of BGAV on the energy dissipation of the ESO/BGAV material was further investigated through tear tests (Fig. 3f). A significant enhancement in tear strength was observed for ESO/BGAV-3 (10.63 N mm^{-1}), outperforming the value of ESO/BGAV-1 (3.71 N mm^{-1}) by 1.87 times. The tearing energy of ESO/BGAV-3 (65.03 kJ m^{-2}) obtained by tearing curve integration was 1.85 times higher than that of ESO/BGAV-1 (22.78 kJ m^{-2}). This was because increasing the BGAV content promoted the epoxy ring-opening reaction between BGAV and ESO, which generated more hydroxyl groups and thereby facilitated the formation of more H-bonds within the polymer network. High-density H-bond crosslinking induced the spatial folding of the flexible ESO chains within the polymer, thereby enhancing the tear resistance of the polymer network.[40]

The fracture morphology of the ESO/BGAV following the tensile test was examined using SEM to analyze its mechanical reinforcement mechanism. As shown in Fig. 3g, the cross-section of ESO/BGAV-1 exhibited loose morphology and many holes, which indicated a low cross-linking density and an unstable internal polymer network for the ESO/BGAV-1 with a smaller BGAV content.[41] In comparison, the ESO/BGAV-2 and ESO/BGAV-4 samples exhibited crack branching and crack deflection and became more continuous, suggesting that increasing the BGAV content effectively suppressed crack propagation in the polymer.[42,43] Interestingly, the ESO/BGAV-3 sample exhibited crack bridging and fiber pull-out characteristics, suggesting that it possessed a stable cross-linking network and excellent energy dissipation capability.[44] However, the fracture surface of ESO/BGAV-5 displayed straight and smooth cracks, which were caused by excessive BGAV leading to over-rigidity of the polymer network and local stress concentration, thereby accelerating stress damage and resulting in brittle fracture.[45] Therefore, the strengthening and toughening mechanisms of ESO/BGAV were illustrated in Fig. 3h. (i) The BGAV with multiple aromatic rings served as a rigid filler and constructed a polyarylation-enhanced bio-based dynamic network with ESO by inducing the formation of H-bonds and dynamic imine bonds, which enhanced the structural stability and mechanical strength of the material.[46,47] (ii) The abundant H-bonds in the system acted as sacrificial bonds, facilitating the dissipation of stress energy in the polymer matrix during tensile deformation.[39] Concurrently, the dense H-bond crosslinking induced folding of the flexible ESO molecular chains, which underwent elastic deformation during stretching. Thus, the toughness of the polymer was improved.[48] (iii) As the stress

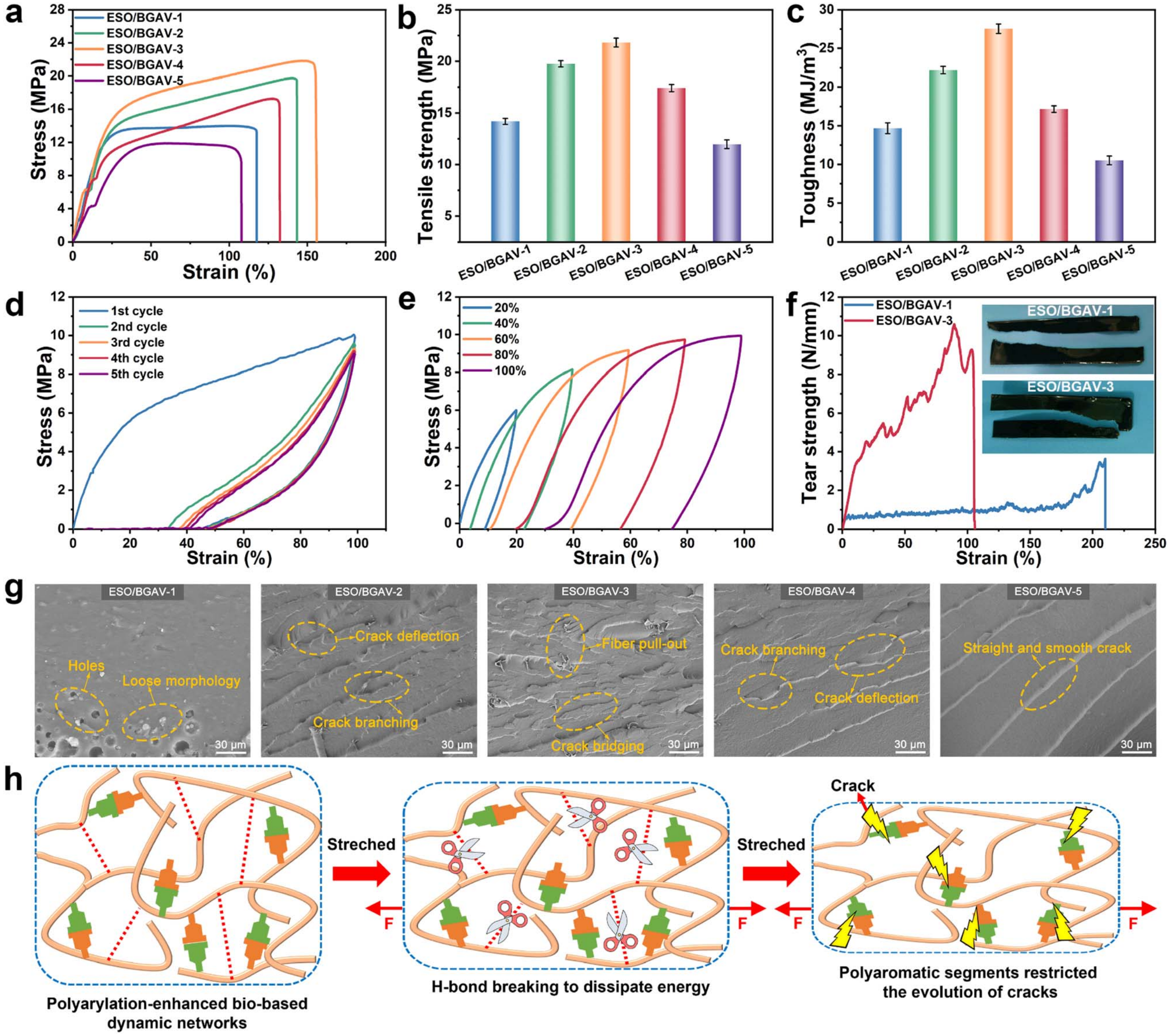

Fig. 3 (a) Tensile stress–strain curves, (b) tensile strength, and (c) toughness of different ESO/BGAV epoxy vitrimers. (d) Cyclic tensile curves and (e) hysteresis curves at different strains of ESO/BGAV-3. (f) Tearing strength–strain curves of ESO/BGAV-1 and ESO/BGAV-3, and pictures of samples after testing. (g) SEM images of the fracture morphology of various ESO/BGAV epoxy vitrimers. (h) Mechanical reinforcement mechanism of ESO/BGAV epoxy vitrimers.

increased further during stretching, cracks gradually initiated within the polymer network. At this stage, the rigid polyaromatic segments in the network inhibited crack propagation through effects such as crack branching, crack deflection, and crack bridging, thereby further enhancing the strength and toughness of the polymer.[31,49]

3.3. Photothermal performances and self-healing properties of ESO/BGAV film

The photothermal performances of the ESO/BGAV film were measured through a home-made photothermal test setup (Fig. 4a). Under the infrared laser source irradiation (1 W cm^{-2}), an infrared camera detected rapid photothermal conversion on the surface of ESO/BGAV-3 (optimal ratio in ESO/BGAV) (Fig. 4b). The surface temperature of the material rose rapidly, reaching 150 °C within 60 seconds and ultimately reaching a maximum of 167 °C (Fig. 4c). The excellent photothermal conversion capability of the ESO/BGAV-3 resulted from the plentiful conjugated structures and strong π–π interactions within the polymer network formed by the polyaromatic segments of BGAV.[14] These conjugated structures promoted electron energy-level transitions, facilitating the release of near-infrared light energy absorbed by the polyaromatic segments *via* non-radiative transitions.[50]

The self-healing properties of the ESO/BGAV were further evaluated. The scratched ESO/BGAV-3 (optimal ratio in ESO/BGAV) film was irradiated under a 1 W cm^{-2} infrared laser source for 10 minutes, and its self-healing process was observed

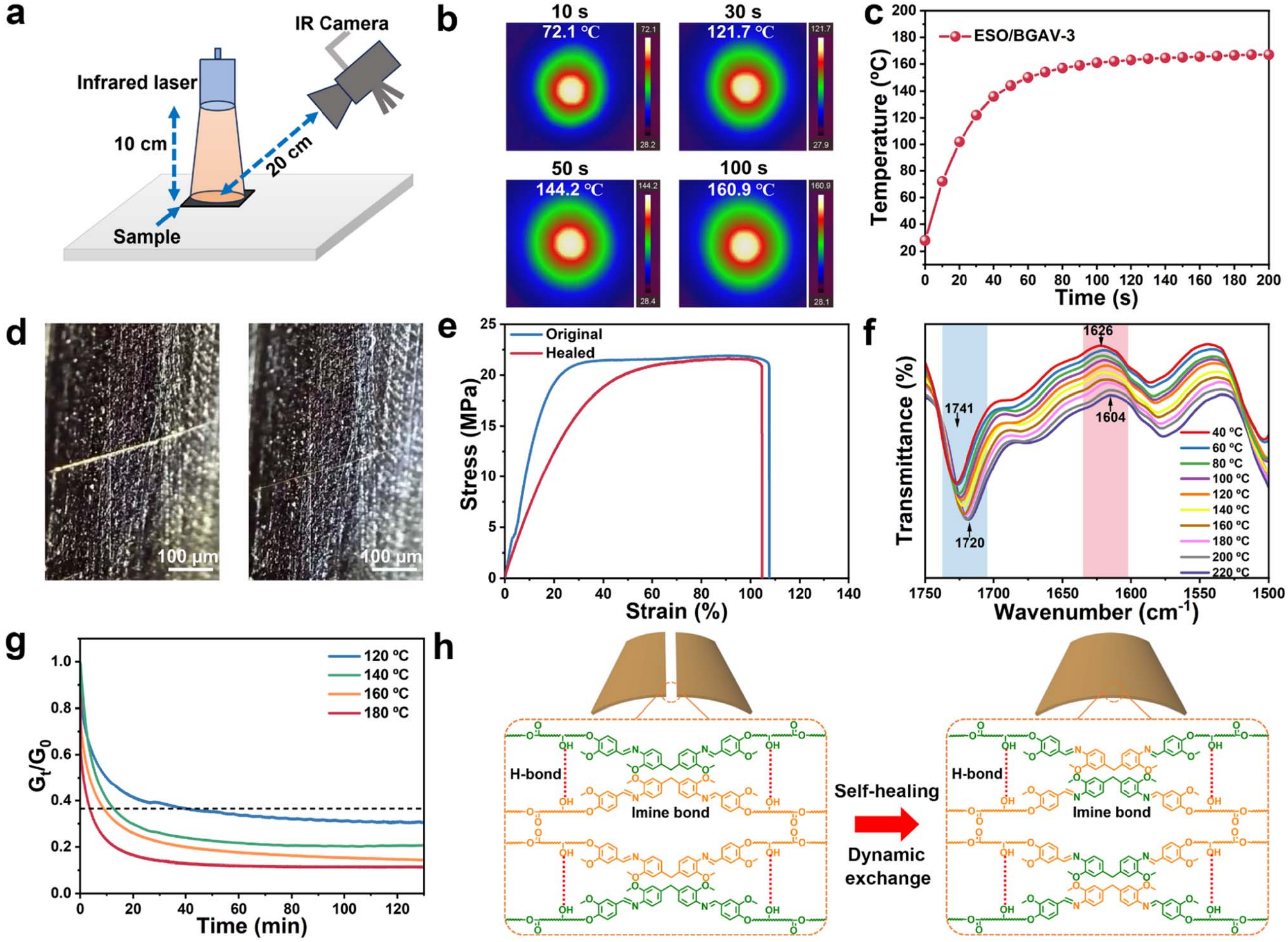

Fig. 4 (a) Schematic illustration of the photothermal test. (b) The infrared images and (c) temperature curve of ESO/BGAV-3 under the infrared laser source. (d) Images of scratched ESO/BGAV-3 before and after self-healing, and (e) the corresponding tensile stress–strain curves. (f) Temperature-dependent FTIR spectra of ESO/BGAV-3 from 40 to 220 °C. (g) Stress relaxation of ESO/BGAV-3 from 120 to 180 °C. (h) Schematic illustration of the self-healing mechanism of ESO/BGAV vitrimer.

with an optical microscope. As shown in Fig. 4d, the scratched area on the surface of the sample had almost completely disappeared after 10 minutes of irradiation. To measure the healing efficiency of the ESO/BGAV-3, the mechanical properties of the healed ESO/BGAV-3 film sample were measured and compared with its original properties. As shown in Fig. 4e, the tensile strength of the healed sample reached 21.53 MPa, which was very close to its original value. The self-healing efficiency of the sample was calculated to be 98.72%, suggesting its favorable self-healing properties. Additionally, the storage modulus of scratched ESO/BGAV-3 after self-healing was measured to calculate its crosslinking density (Fig. S8). The crosslinking density of healed ESO/BGAV-3 was 9056.98, which reached 92.67% of the crosslinking density of the initial ESO/BGAV-3. This result further demonstrated the remarkable self-healing properties of ESO/BGAV-3. The mechanism of self-healing properties in ESO/BGAV was investigated using temperature-dependent FTIR and stress relaxation tests. The temperature-dependent FTIR spectra of ESO/BGAV-3 are shown in Fig. 4f. As the temperature increased, the characteristic peak of the C═N group in the spectrum shifted from 1626 cm^{-1} to 1604 cm^{-1}, which indicated that the dynamic imine bonds in the polymer network gradually underwent dissociation under high temperatures.[51] Furthermore, the ester carbonyl peak in the spectrum shifted from 1741 cm^{-1} to 1720 cm^{-1}, which suggested that the dynamic H-bonds in the network had also dissociated through thermal action.[52] The stress relaxation curves of ESO/BGAV-3 in the range of 120–180 °C were shown in Fig. 4g. In the Maxwell model of viscoelastic fluid, the relaxation time referred to the duration of the process of relaxing to $1/e$ of the original modulus.[51] The relaxation time of the polymer decreased from 2278 s at 120 °C to 215 s at 180 °C with increasing temperature, which was because high temperatures increased the mobility of the molecular chains in the polymer, thereby promoting the exchange and rearrangement of dynamic imine bonds and H-bonds within the network. A linear relationship between the stress relaxation time and $1000/T$ was established based on the Arrhenius equation (Fig. S9), from which an activation energy (E_a) of 56.2 kJ mol^{-1} was calculated. Therefore, the self-healing mechanism of the ESO/BGAV was summarized in Fig. 4h. A bio-based dynamic network with abundant imine bonds and H-bonds was constructed from ESO and BGAV. The BGAV containing polyaromatic segments and conjugated structures could absorb near-infrared light energy and convert it into heat energy.[14] Driven by heat energy, the dynamic exchange and reconstruction of reversible imine bonds and H-bonds within the network promoted the self-healing of polymer wounds.[15]

3.4. Recyclability of ESO/BGAV film

The recycling of polymers is an essential approach to achieving their sustainability. To assess the recyclability of the ESO/BGAV film, its physical and chemical recycling tests were conducted. The physical recycling process of ESO/BGAV-3 (optimal ratio in ESO/BGAV) is shown in Fig. 5a. The prepared ESO/BGAV-3 film was mechanically ground into powder and subsequently hot-pressed at 140 °C to form a physically recycled film. The tensile strength of the physically recycled ESO/BGAV-3 film was measured and compared with its original value to calculate the physical recycling rate. The tensile strength of the physically recycled ESO/BGAV-3 film reached 20.79 MPa (Fig. 5b), and its physical recycling rate achieved 95.32% (Fig. 5e). The storage modulus of ESO/BGAV-3 after physical recycling was measured (Fig. S10a), and its crosslinking density was calculated to be 8359.16. This value reached 85.53% of the crosslinking density of the initial ESO/BGAV-3. These results illustrated the extraordinary physical recyclability of the ESO/BGAV-3, which was attributed to the thermal-responsive reversible reconstruction of its dynamic polymer network.[20] The chemical recycling process of ESO/BGAV-3 is illustrated in Fig. 5c. The prepared ESO/BGAV-3 film was immersed in a mixed chemical solvent (CH_2Cl_2/THF/HCl) and shaken at 25 °C for 6 hours to form a depolymerized ESO/BGAV solution. The chemically recycled film was recovered from the depolymerized ESO/BGAV solution after desolvation and curing. The tensile strength of the chemically recycled ESO/BGAV-3 film was measured and compared with its original value to calculate the chemical recycling rate. The tensile strength of the chemically recycled ESO/BGAV-3 film reached 21.27 MPa (Fig. 5d), and its chemical recycling rate reached 97.52% (Fig. 5e). The storage modulus of ESO/BGAV-3 after chemical recycling was measured to calculate its crosslinking density (Fig. S10b), which was determined to be 8821.44. This value was 90.26% of the crosslinking density of the initial ESO/BGAV-3, suggesting the exceptional chemical recyclability of ESO/BGAV-3. The chemical structure of the depolymerized ESO/BGAV-3 solution was analyzed using ^{1}H NMR spectroscopy. As shown in Fig. 5f, the characteristic peak at 4.95 ppm corresponding to the amine groups of the BGA and the characteristic peak at 9.71 ppm corresponding to the aldehyde groups of the vanillin were observed on the spectrum of the depolymerized ESO/BGAV-3. This indicated that the reversible imine bond in ESO/BGAV-3 was opened during depolymerization in the chemical mixed solvent, regenerating amine and aldehyde groups. These groups were subsequently utilized for the dynamic reconstruction of the recycled film, which imparted the material with favorable chemical recyclability.

3.5. Adhesion performance, bonding performance, and water resistance of ESO/BGAV adhesive

The bonding performance of ESO/BGAV epoxy vitrimer as a bio-based adhesive was studied. The ESO/BGAV-3 (optimal ratio in

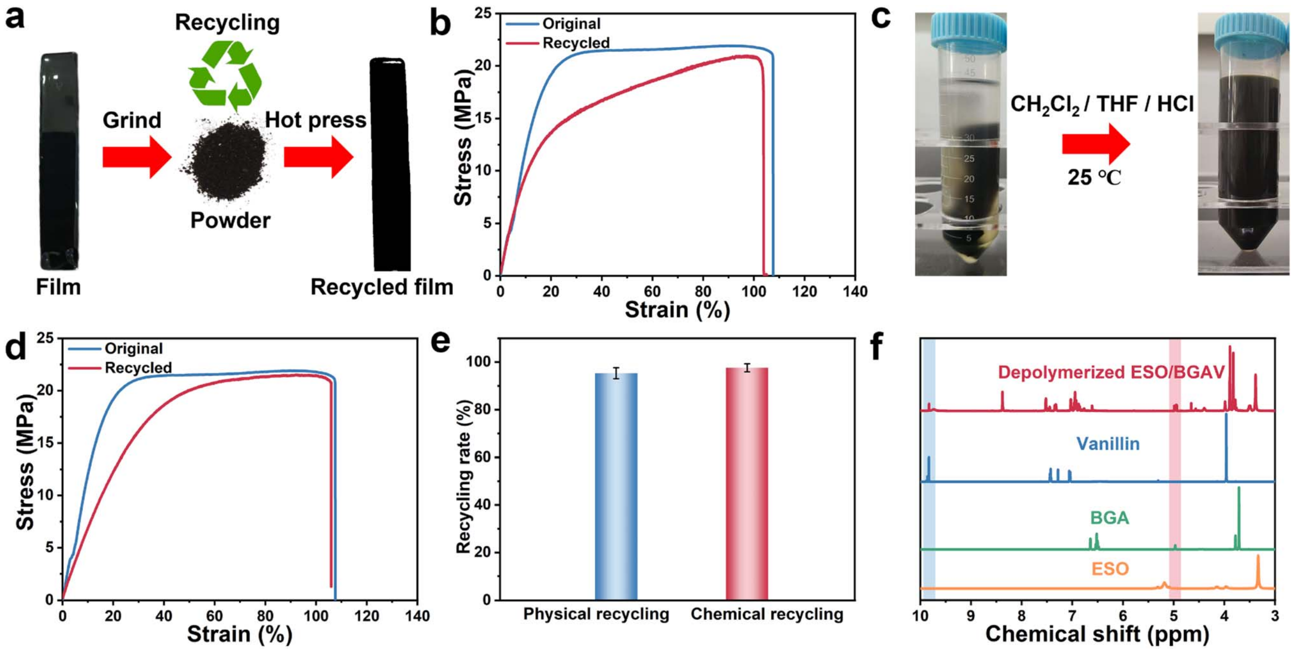

Fig. 5 (a) Physical recycling process of ESO/BGAV-3 film. (b) Tensile stress–strain curves of original and physically recycled ESO/BGAV-3 film. (c) Chemical recycling process of ESO/BGAV-3 film. (d) Tensile stress–strain curves of original and chemically recycled ESO/BGAV-3 film. (e) Physical recycling rate and chemical recycling rate of ESO/BGAV-3 film. (f) ^{1}H NMR spectra of depolymerized ESO/BGAV-3 solution and vanillin, BGA, and ESO.

ESO/BGAV) exhibited robust adhesion to a wide range of substrates at room temperature, including organic materials such as rubber, wood, and PTFE, as well as inorganic materials like ceramics, stainless steel (SS), and glass (Fig. 6a). The adhesion strength of the ESO/BGAV-3 on various substrates at room temperature was measured through lap shear tests (Fig. 6b). The ESO/BGAV-3 represented outstanding adhesion strength of 86.04, 136.75, 324.69, 460.83, 366.07, 670.41, 1082.35, 938.40, 1026.73, and 794.86 kPa for PTFE, glass, PE, PMMA, PP, rubber, iron, copper, aluminum, and wood, respectively. Moreover, the bonding strength of a series of ESO/BGAV adhesives on iron, copper, aluminum, and wood after thermal curing was measured. As shown in Fig. 6c–f, the bonding strengths of ESO/BGAV-1 for iron, copper, aluminum, and wood achieved 11.17, 8.37, 9.16, and 4.47 MP, respectively. However, the bonding strength of ESO/BGAV increased initially and then decreased with increasing BGAV content. The bonding strengths of ESO/BGAV-3 for iron, copper, aluminum, and wood reached 15.18, 12.93, 13.91, and 7.31 MP, respectively, which represented an increase in strength of 35.90%, 54.48%, 51.86%,

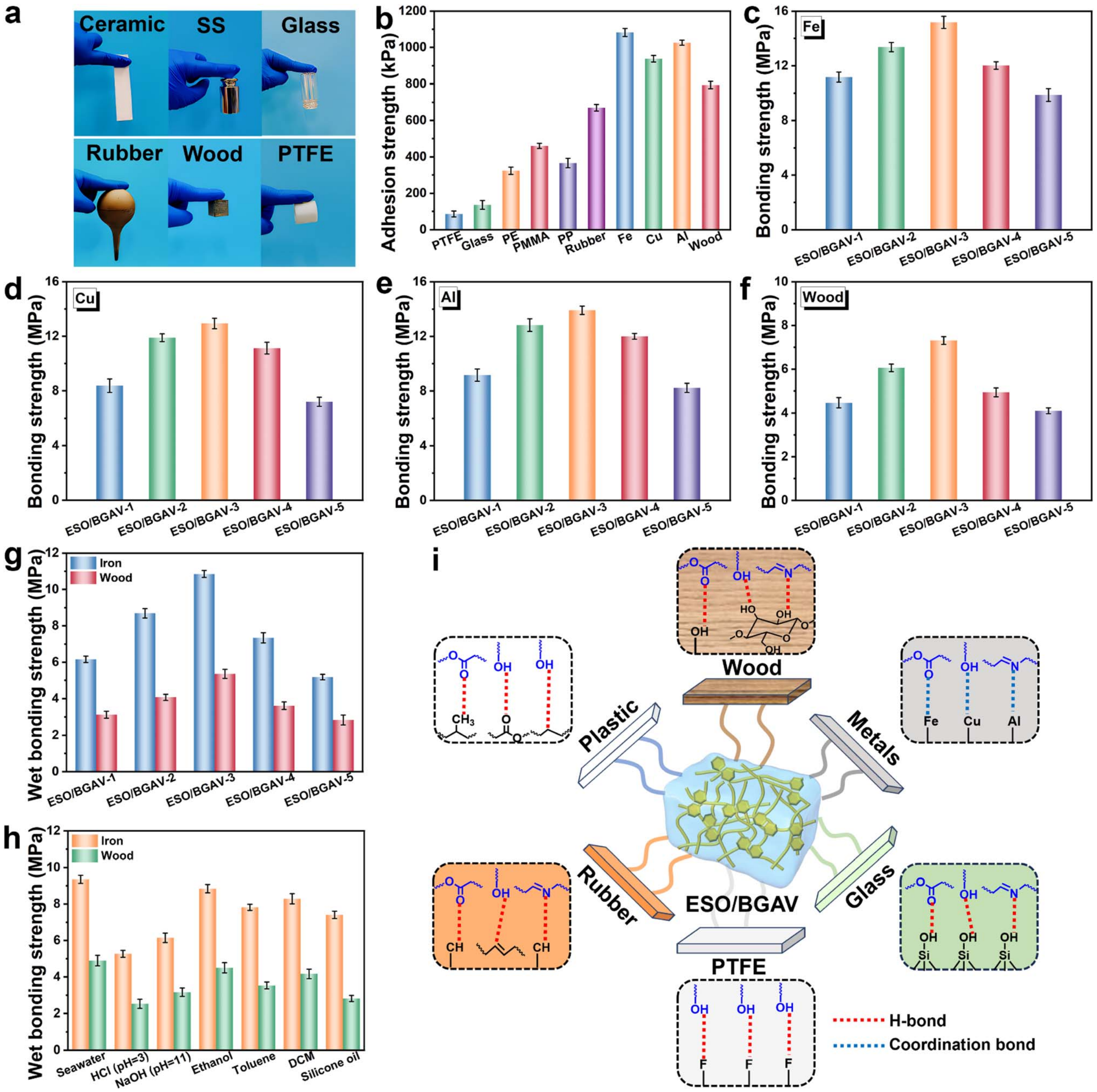

Fig. 6 (a) Pictures for adhesion properties of ESO/BGAV-3 adhesive on diverse substrates. (b) Bonding strength of different ESO/BGAV adhesives on (c) iron, (d) copper, (e) aluminum, and (f) wood. (g) Water-resistant wet bonding strength of different ESO/BGAV adhesives on iron and wood. (h) Solvent-resistant wet bonding strength of ESO/BGAV-3 adhesive on iron and wood. (i) Schematic illustration of the bonding enhancement mechanism of the ESO/BGAV on different substrates.

and 63.53% compared to those of ESO/BGAV-1. The enhancement in bonding strength was ascribed to the improved cohesive force of the ESO/BGAV and its interfacial interaction with the substrates, which was achieved by incorporating higher BGAV content.[53] Excessive BGAV could disrupt the crosslinking network and reduce structural stability. As a result, the bonding strength of ESO/BGAV-5 for iron, copper, aluminum, and wood decreased to 9.86, 7.21, 8.23, and 4.10 MPa, respectively. Besides, the series of ESO/BGAV adhesives demonstrated bonding strength on wood that surpassed that of petroleum-based phenolic resin (1.70 MPa), urea-formaldehyde resin (1.94 MPa), and other reported bio-based adhesives (Table S2), which demonstrated significant potential for replacing petroleum-based adhesives. The enhancement mechanism of the bonding performance was illustrated in Fig. 6i. The bonding strength of adhesives was primarily determined by both the internal cohesive force of the adhesive itself and the interfacial adhesion force between the adhesive and the substrates. ESO and BGAV formed a stable cross-linked network.[40] The rigid polyaromatic segments and the abundant imine and H-bonds within the network enhanced the cohesive force of the adhesive.[54] Furthermore, the carbonyl, hydroxyl, and imine groups of the adhesive could form H-bonds and coordination bonds with various substrates, which improved the interfacial adhesion to these substrates.[53] Thus, ESO/BGAV achieved a balance between cohesive force and interfacial adhesive force, resulting in exceptional bonding performance.

The water resistance of ESO/BGAV epoxy vitrimers as bio-based adhesives was further investigated by measuring their wet bonding strength on iron and wood. As shown in Fig. 6g, the wet bonding strength of ESO/BGAV exhibited an initial increase followed by a decrease with increasing the additional amount of BGAV. The wet bonding strength of ESO/BGAV-3 (optimal ratio in ESO/BGAV) on iron and wood reached the maximum values of 10.85 and 5.36 MPa, which represented an increase in bonding strength of 76.14% and 70.16% on iron and wood, respectively, compared with those of ESO/BGAV-1 (6.16 and 3.15 MPa). This was because increasing the BGAV content raised the number of polyaromatic segments in the network, leading to the formation of more stable hydrophobic structures that inhibited water damage.[36] Meanwhile, the dynamic imine bonds and H-bonds introduced by BGAV facilitated the folding and densification of the ESO molecular chains, further hindering water intrusion.[31] However, excessive BGAV compromised the integrity and stability of the crosslinking structure of adhesives, resulting in reduced hydrophobicity. Thus, the wet bonding strength of ESO/BGAV-5 on iron and wood decreased to 5.18 and 2.84 MPa. Besides, the wet bonding strength of all ESO/BGAV adhesives met the criteria for manufacturing wood-based panels (≥0.70 MPa). Interestingly, the ESO/BGAV-3 adhesive possessed excellent resistance to different solvents (Fig. 6h). The wet bonding strength of ESO/BGAV-3 on iron and wood in seawater, HCl solution (pH = 3), NaOH solution (pH = 11), ethanol, toluene, DCM, and silicone oil can reach from 2.53 MPa to 9.35 MPa. Additionally, different ESO/BGAV films retained a residual mass greater than 88% and 85% after 7 days of immersion in ethyl acetate and DCM, respectively (Fig. S11). This favorable solvent adaptability was attributed to the robust polyarylation dynamic network and abundant interfacial interactions, which endowed the adhesive with structural stability and interfacial adhesion in various solvent environments.[16,40]

3.6. Recyclability and antimicrobial properties of ESO/BGAV adhesive

The rebonding of adhesives after adhesive failure and their recycling and reuse after depolymerization are crucial for improving their practical application value. The ESO/BGAV adhesive exhibited excellent recyclability based on its dynamic adaptive characteristics. Fig. 7a demonstrated the physical recycling and reprocessing process of the ESO/BGAV adhesive. The two separated iron substrates coated by ESO/BGAV-3 (optimal ratio in ESO/BGAV) after lap shear tests could be recycled and rebonded through heating. The bonding strength of the rebonded iron substrates was tested over three cycles and compared with the original value of the ESO/BGAV-3 on iron substrates for calculating the physical recycling. As shown in Fig. 7b, the first, second, and third recycled bonding strengths of the ESO/BGAV-3 on iron substrates after physical recycling were 14.83, 14.45, and 14.16 MPa, and the corresponding first, second, and third recycling rates were 97.69%, 95.32%, and 93.28% (Fig. 7c). The outstanding physical recyclability of the adhesive resulted from the dynamic exchange of internal reversible covalent bonds and the reconstruction of interfacial coordination bonds activated by thermal energy.[14,16] Furthermore, the chemical recycling and reprocessing process of the ESO/BGAV adhesive is shown in Fig. 7d. The iron substrate specimens bonded with the ESO/BGAV-3 adhesive could be debonded using a mixed chemical solvent (CH_2Cl_2/THF/HCl), and the recycled ESO/BGAV-3 adhesive was obtained through further desolvation. The recycled adhesive could reconstruct the dynamic polymer network after thermal curing. The bonding strength of the chemically recycled ESO/BGAV-3 adhesive on iron substrates was evaluated over three cycles and compared with the original value of the ESO/BGAV-3 on iron substrates to calculate the chemical recycling rate. As shown in Fig. 7e, the first, second, and third recycled bonding strengths of the ESO/BGAV-3 on iron substrates after chemical recycling were 14.61, 14.22, and 13.96 MPa, and the corresponding first, second, and third recycling rates were 96.25%, 93.68%, and 91.96% (Fig. 7f). The exceptional chemical recyclability was attributed to the depolymerization induced by the mixed chemical solvent, which broke the dynamic imine bonds within the polymer and the coordination bonds at the bonding interface. Following further curing and crosslinking, dynamic imine bonds were re-formed within the polymer network, while interfacial rearrangement of molecular chains drove the recombination of coordination bonds at the bonding interface.[55]

Bio-based adhesives are susceptible to microbial erosion, so enhancing their antibacterial properties and mold resistance is vital for extending the service life of the adhesives. The antibacterial properties of the ESO/BGAV adhesive were evaluated using *E. coli* and *S. aureus*. As shown in Fig. 7g, compared with the control group, the samples treated with the ESO/BGAV-3

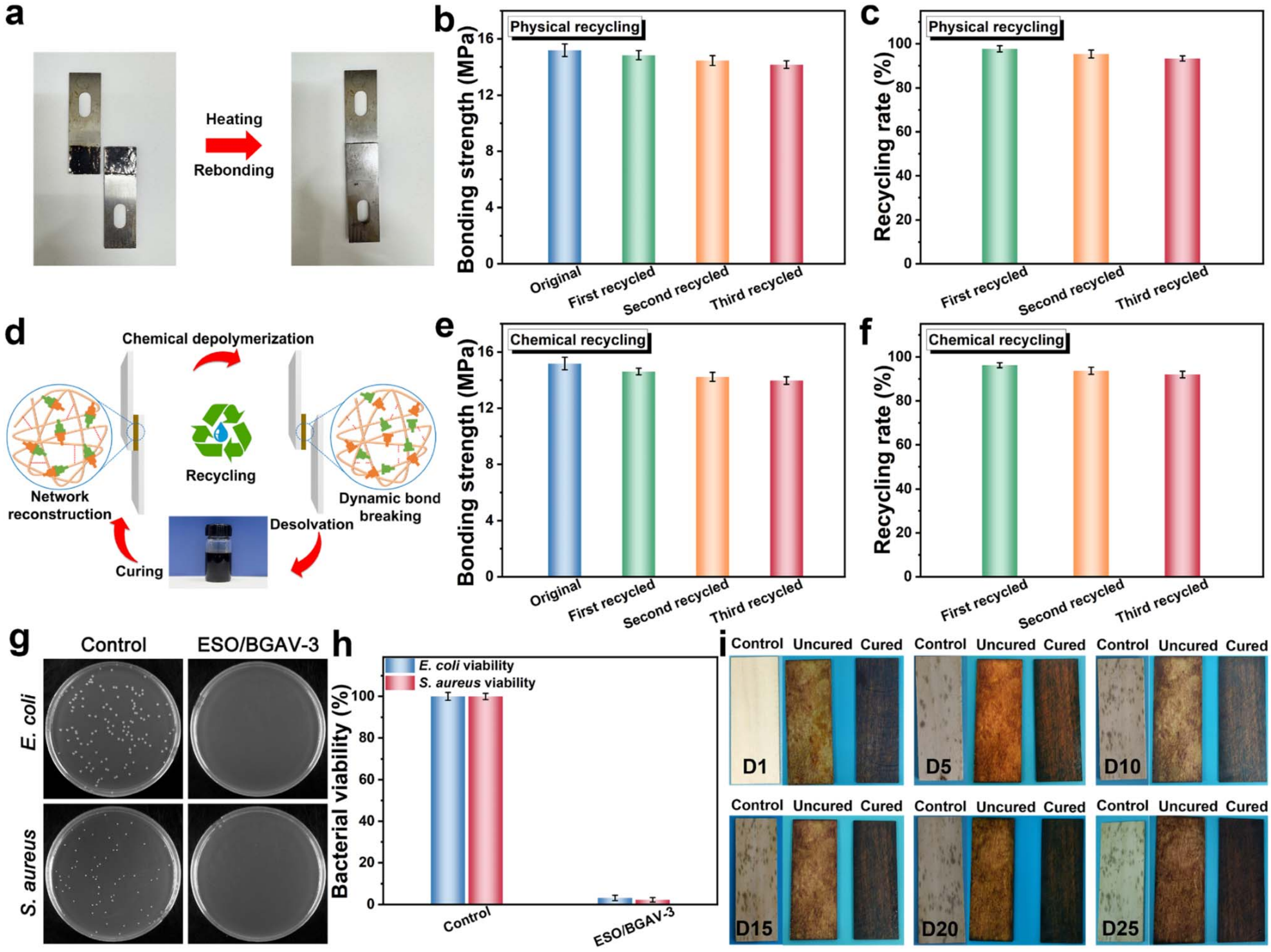

Fig. 7 (a) Physical recycling and reprocessing process of the ESO/BGAV-3 adhesive. (b) Bonding strength of the original and physically recycled ESO/BGAV-3 adhesive after different recycling cycles. (c) Physical recycling rate of ESO/BGAV-3 adhesive. (d) Chemical recycling and reprocessing process of the ESO/BGAV-3 adhesive. (e) Bonding strength of the original and chemically recycled ESO/BGAV-3 adhesive after different recycling cycles. (f) Chemical recycling rate of ESO/BGAV-3 adhesive. (g) Images of the surviving *E. coli* and *S. aureus* colonies and (h) corresponding bacterial viability after treatment without and with ESO/BGAV-3 adhesive. (i) Assessment of mold growth resistance of wood veneers coated with uncured and cured ESO/BGAV-3 adhesive.

(optimal ratio in ESO/BGAV) showed almost no surviving bacterial colonies. The bacterial viability of the samples treated with ESO/BGAV-3 decreased significantly relative to the control group, with survival rates of only 3.17% for *E. coli* and 2.29% for *S. aureus* (Fig. 7h). The effective antibacterial properties resulted from the ability of the dynamic imine bonds in the polymer to disrupt the bacterial cell membrane structure, thus affecting its permeability and ultimately leading to bacterial death.[47,56] The mold resistance of the ESO/BGAV adhesive was evaluated by coating it on wood veneers and storing them at 30 °C and 90% RH. As shown in Fig. 7i, the untreated control wood sample developed extensive brown fungal colonies on the surface after 5 days, and the colonies gradually increased over time. In comparison, the wood sample coated by uncured ESO/BGAV-3 presented no signs of mold growth even after 25 days of storage, which was attributed to the inhibitory effect of the imine bonds in the polymer on mold growth.[47,56] The excellent mold resistance of the uncured adhesive helped extend its shelf life. Moreover, no mold growth was detected on the surface of the wood sample coated with the cured adhesive after 25 days of storage. This result further demonstrated the long-term mold resistance efficacy of the cured adhesive, which helped prevent the erosion of the cured adhesive layer by mold during its service life.

4. Conclusions

In conclusion, we successfully prepared a strong, tough, recyclable, and multifunctional bio-based epoxy vitrimer *via* ESO and lignin-based aromatic monomers of vanillyl alcohol, guaiacol, and vanillin. These lignin-based aromatic monomers served as bio-based aromatic building blocks to synthesize the BGAV with dynamic imine bonds, which was then used as a curing agent for ESO to construct a bio-based epoxy vitrimer with a dynamic network. BGAV enhanced the stability of the polymer network by forming rigid polyaromatic segments, and thus the epoxy vitrimer exhibited a high mechanical strength of 21.81 MPa. Additionally, the H-bonds in the network improved the energy dissipation of the polymer by acting as sacrificial bonds, and thus the epoxy vitrimer possessed excellent toughness of 27.53 MJ m^{-3}. Moreover, the vitrimer achieved significant self-healing properties and recyclability through the reversible reorganization of dynamic imine bonds within the network. Besides, this vitrimer had favorable antibacterial properties and mold resistance owing to the antimicrobial action of the imine bonds. Furthermore, the polyaromatic segments provided the polymer network with conjugated structures and hydrophobic groups, thereby causing remarkable photothermal conversion performance and water resistance for the vitrimer. Impressively, this vitrimer as a bio-based adhesive demonstrated outstanding bonding performance based on a balance between the internal cohesive force of the polymer and the adhesive force at the bonding interface induced by the dynamic network, and the bonding strength could reach 15.18 MPa. This study offers an effective strategy for creating a bio-based epoxy vitrimer that simultaneously possesses exceptional mechanical properties, recyclability, and other functionalities, exhibiting great promise for advancing the development of sustainable bio-based epoxy resins.

Author contributions

Zhiwei Chang: methodology, data curation, writing-original draft, writing-review & editing, project administration; Xiaochun Bao: conceptualization, validation, formal analysis; Guimin Yuan: investigation, software, resources; Yuang Ma: visualization, investigation; Ming Li: supervision, project administration; Hanjie Ying: supervision.

Conflicts of interest

The authors declare no conflict of interest.

Data availability

The data of this study are available from the corresponding author upon reasonable request.

Supplementary information: Fig. S1. Dimensions of the specimen for adhesion performance, bonding performance, and water resistance measurements. Fig. S2. ^{1}H nuclear magnetic resonance (NMR) spectra of (a) BGF, (b) ABGF, (c) BGA, (d) BGAV. Fig. S3. X-ray photoelectron spectroscopy (XPS) spectra of ESO, BGAV, and ESO/BGAV. Fig. S4. The crosslinking density of different ESO/BGAV epoxy vitrimers. Fig. S5. Loss tangent ($\tan\delta$) of different ESO/BGAV epoxy vitrimers. Fig. S6. Swelling ratio of different ESO/BGAV epoxy vitrimers. Fig. S7. Hysteresis loss per cycle at different strains. Fig. S8. Storage modulus of scratched ESO/BGAV-3 after self-healing. Fig. S9. Linear fitting curve based on the Arrhenius equation ($R^2 = 0.9902$). Fig. S10. Storage modulus of ESO/BGAV-3 after (a) physical recycling and (b) chemical recycling. Fig. S11. Change in the residual weight of different ESO/BGAV films with immersion time. Table S1. Formulations of the ESO/BGAV-1, ESO/BGAV-2, ESO/BGAV-3, ESO/BGAV-4, and ESO/BGAV-5. Table S2. Comparison of bonding strength and wet bonding strength of the ESO/BGAV adhesive with phenolic resin, urea-formaldehyde resin, and other reported bio-based adhesives on wood substrate. See DOI: **https://doi.org/10.1039/d5ra06660c**.

Acknowledgements

This research was supported by the National Natural Science Foundation of China (Grant No. 22478182), and the Natural Science Foundation of the Jiangsu Higher Education Institutions (Grant No. 24KJB530013).

References

1 R. Auvergne, S. Caillol, G. David, B. Boutevin and J. P. Pascault, *Chem. Rev.*, 2014, **114**, 1082–1115.
2 J. K. Liu, S. P. Wang, Y. Y. Peng, J. Zhu, W. W. Zhao and X. Q. Liu, *Prog. Polym. Sci.*, 2021, **113**, 101353.
3 X. Wang, H. X. Niu, W. W. Guo, L. Song and Y. Hu, *Chem. Eng. J.*, 2021, **421**, 129738.
4 Y. Hu, S. Y. Tong, Y. Sha, J. Yu, L. H. Hu, Q. Huang, P. Y. Jia and Y. H. Zhou, *Chem. Eng. J.*, 2023, **471**, 144633.
5 X. Wang, E. N. Kalali and D. Y. Wang, *ACS Sustainable Chem. Eng.*, 2015, **3**, 3281–3290.
6 C. H. Chen, S. H. Tung, R. J. Jeng, M. M. Abu-Omar and C. H. Lin, *Green Chem.*, 2019, **21**, 4475–4488.
7 P. Yang, W. R. Li and Q. Y. Zhan, *ACS Sustainable Chem. Eng.*, 2023, **11**, 1200–1206.
8 G. Q. Zhu, J. S. Zhang, J. Huang, Y. H. Qiu, M. T. Liu, J. N. Yu, C. G. Liu, Q. Q. Shang, Y. Hu, L. H. Hu and Y. H. Zhou, *Chem. Eng. J.*, 2023, **452**, 139401.
9 J. N. Xin, M. Li, R. Li, M. P. Wolcott and J. W. Zhang, *ACS Sustainable Chem. Eng.*, 2016, **4**, 2754–2761.
10 C. R. Westerman, B. C. McGill and J. J. Wilker, *Nature*, 2023, **621**, 306–311.
11 M. Qi, Y. J. Xu, W. H. Rao, X. Luo, L. Chen and Y. Z. Wang, *RSC Adv.*, 2018, **8**, 26948–26958.
12 H. Jiang, L. Sun, Y. R. Zhang, Q. Q. Liu, C. Y. Ru, W. X. Zhang and C. J. Zhao, *Polym. Degrad. Stab.*, 2019, **160**, 45–52.
13 N. Zheng, Y. Xu, Q. Zhao and T. Xie, *Chem. Rev.*, 2021, **121**, 1716–1745.
14 Y. F. Yang, H. Zhou, X. Q. Chen, T. T. Liu, Y. Zheng, L. Dai and C. L. Si, *Chem. Eng. J.*, 2023, **477**, 147216.
15 Z. Q. Zhang, D. Lei, C. X. Zhang, Z. Y. Wang, Y. H. Jin, W. Zhang, X. K. Liu and J. Q. Sun, *Adv. Mater.*, 2023, **35**, 2208619.
16 Y. B. Fu, S. Chen, X. Y. Chen, H. X. Zheng, X. L. Yan, Z. L. Liu, M. T. Wang and L. Liu, *Adv. Funct. Mater.*, 2024, **34**, 2314561.
17 B. Yang, T. T. Ni, J. J. Wu, Z. Z. Fang, K. X. Yang, B. He, X. Q. Pu, G. C. Chen, C. J. Ni, D. Chen, Q. Zhao, W. Li, S. J. Li, H. Li, N. Zheng and T. Xie, *Science*, 2025, **388**, 170–175.
18 N. Yang, Y. Jiang, Q. W. Tan, J. H. Ma, D. Z. Zhan, Z. H. Wang, X. Wang, D. H. Zhang and N. Hadjichristidis, *Angew. Chem., Int. Ed.*, 2022, **61**, e202211713.

19 Y. Hu, P. Y. Jia, M. E. Lamm, Y. Sha, L. B. Kurnaz, Y. F. Ma and Y. H. Zhou, *Composites, Part B*, 2023, **259**, 110704.

20 X. Z. Wang, X. B. Huang, Z. M. Ji, H. Q. Sheng and H. Liu, *ACS Sustainable Chem. Eng.*, 2024, **12**, 7147–7157.

21 Y. Ito, D. Aoki and H. Otsuka, *Polym. Chem.*, 2020, **11**, 5356–5364.

22 S. Q. Huo, T. Sai, S. Y. Ran, Z. H. Guo, Z. P. Fang, P. G. Song and H. Wang, *Composites, Part B*, 2022, **234**, 109701.

23 X. W. Jiao, Y. N. Ma, Z. H. Zhao, L. Gao, B. Y. Zhang, J. G. Yang, M. H. Li and J. Hu, *Adv. Funct. Mater.*, 2024, **34**, 2409223.

24 J. Li, B. Y. Zhang, X. J. Zhang, Y. X. Li, K. X. Li, T. Y. Wang and X. W. Li, *Small*, 2025, **21**, 2407579.

25 Z. H. Chen, X. W. Peng, Z. X. Chen, T. Z. Li, R. Zou, G. Shi, Y. F. Huang, P. Cui, J. Yu, Y. L. Chen, X. Chi, K. P. Loh, Z. Q. Liu, X. H. Li, L. X. Zhong and J. Lu, *Adv. Mater.*, 2023, **35**, 2209948.

26 A. K. Deepa and P. L. Dhepe, *RSC Adv.*, 2014, **4**, 12625–12629.

27 S. K. Singh and J. D. Ekhe, *RSC Adv.*, 2014, **4**, 27971–27978.

28 S. Lemouzy, A. Delavarde, F. Lamaty, X. Bantreil, J. Pinaud and S. Caillol, *Green Chem.*, 2023, **25**, 4833–4839.

29 Y. X. Hao, L. Y. Zhong, T. C. Li, J. H. Zhang and D. H. Zhang, *ACS Sustainable Chem. Eng.*, 2023, **11**, 11077–11087.

30 X. Y. Jian, Y. He, Y. D. Li, M. Wang and J. B. Zeng, *Chem. Eng. J.*, 2017, **326**, 875–885.

31 Z. W. Chang, Y. L. Shen, J. F. Xue, Y. Sun and S. F. Zhang, *Chem. Eng. J.*, 2023, **457**, 140984.

32 Y. Zhou, J. Luo, Q. M. Jing, S. B. Ge, S. Chen, Z. H. Guo, J. Z. Li, Z. X. Liu, P. He, X. M. He and B. B. Xu, *Adv. Funct. Mater.*, 2024, **34**, 2406557.

33 W. D. Gu, F. Li, X. R. Liu, Q. Gao, S. S. Gong, J. Z. Li and S. Q. Q. Shi, *Green Chem.*, 2020, **22**, 1319–1328.

34 B. X. Zheng, T. Liu, J. Liu, Y. L. Cui, R. X. Ou, C. G. Guo, Z. Z. Liu and Q. W. Wang, *Composites, Part B*, 2023, **257**, 110697.

35 Y. Hu, S. Y. Tong, L. H. Hu, M. Zhang, Q. Huang, Y. Sha, P. Y. Jia and Y. H. Zhou, *Chem. Eng. J.*, 2023, **477**, 147284.

36 Y. X. Li, S. H. Li and J. Q. Sun, *Adv. Mater.*, 2021, **33**, 2007371.

37 Z. H. Yuan, T. Wang, C. Y. Shao, S. R. Yang, W. X. Sun, Y. H. Chen, Z. P. Peng and Z. Tong, *Adv. Funct. Mater.*, 2025, **35**, 2412950.

38 X. Liu, H. H. Wu, W. Xu, Y. Jiang, J. H. Zhang, B. J. Ye, H. J. Zhang, S. F. Chen, M. H. Miao and D. H. Zhang, *Adv. Mater.*, 2024, **36**, 2308434.

39 E. Filippidi, T. R. Cristiani, C. D. Eisenbach, J. H. Waite, J. N. Israelachvili, B. K. Ahn and M. T. Valentine, *Science*, 2017, **358**, 502–505.

40 B. Zhang, P. L. Zhang, G. L. Zhang, C. F. Ma and G. Z. Zhang, *Adv. Mater.*, 2024, **36**, 2313495.

41 Y. T. Xu, Y. F. Han, Y. Li, J. C. Li, J. Z. Li and Q. Gao, *Chem. Eng. J.*, 2022, **437**, 135437.

42 Q. F. Guan, H. B. Yang, Z. M. Han, Z. C. Ling and S. H. Yu, *Nat. Commun.*, 2020, **11**, 5401.

43 Z. W. Chang, Y. L. Shen, J. F. Xue, Y. Sun and S. F. Zhang, *Ind. Crops Prod.*, 2023, **202**, 116992.

44 J. C. C. Yeo, J. K. Muiruri, J. J. Koh, W. Thitsartarn, X. K. Zhang, J. H. Kong, T. T. Lin, Z. B. Li and C. B. He, *Adv. Funct. Mater.*, 2020, **30**, 2001565.

45 J. H. Xu, T. Liu, Y. Z. Zhang, Y. N. Zhang, K. Wu, C. X. Lei, Q. Fu and J. J. Fu, *Matter*, 2021, **4**, 2474–2489.

46 T. Zhao, J. Gao, Y. X. Zheng, J. X. Liu, Y. F. Ni, W. Zhao, Q. B. Guan and Z. W. You, *Adv. Mater.*, 2025, 2510431.

47 J. Y. Peng, S. Y. Xie, T. Liu, D. Y. Wang, R. X. Ou, C. G. Guo, Q. W. Wang and Z. Z. Liu, *Composites, Part B*, 2022, **242**, 110109.

48 X. Fang, N. A. Tian, W. Y. Hu, Y. A. Qing, H. Wang, X. Gao, Y. G. Qin and J. Q. Sun, *Adv. Funct. Mater.*, 2022, **32**, 2208623.

49 L. Liu, M. H. Zhu, X. D. Xu, X. Li, Z. W. Ma, Z. Jiang, A. Pich, H. Wang and P. A. Song, *Adv. Mater.*, 2021, **33**, 2105829.

50 Z. W. Sun, C. Dang, H. M. Zhang, Y. F. Feng, M. Jiang, S. N. Hu, Y. Z. Shao, S. W. Hao, C. Y. Shao, W. Zhai and R. C. Sun, *Adv. Funct. Mater.*, 2024, **34**, 2405130.

51 W. D. Gu, F. Li, T. Liu, S. S. Gong, Q. Gao, J. Z. Li and Z. Fang, *Adv. Sci.*, 2022, **9**, 2103623.

52 X. K. Wu, J. L. Zhang, H. A. Li, H. H. Gao, M. Wu, Z. K. Wang and Z. Wang, *Chem. Eng. J.*, 2023, **454**, 140268.

53 W. X. Zhang, M. Y. Zhu, M. Li, R. J. Hu, Z. W. Chang, C. J. Zhu and H. J. Ying, *ACS Sustainable Chem. Eng.*, 2025, **13**, 8193–8205.

54 R. J. Song, X. Y. Wang, M. Johnson, C. Milne, A. Lesniak-Podsiadlo, Y. H. Li, J. Lyu, Z. S. Li, C. Y. Zhao, L. Z. Yang, I. Lara-Sáez, A. Sigen and W. X. Wang, *Adv. Funct. Mater.*, 2024, **34**, 2313322.

55 Z. H. Wang, B. W. Liu, F. R. Zeng, X. C. Lin, J. Y. Zhang, X. L. Wang, Y. Z. Wang and H. B. Zhao, *Sci. Adv.*, 2022, **8**, eadd8527.

56 X. Jin, Y. H. Xiong, X. Y. Zhang, R. X. Wang, Y. G. Xing, S. Duan, D. F. Chen, W. Tian and F. J. Xu, *Adv. Funct. Mater.*, 2019, **29**, 1807915.